

Interacting Particle Systems Modeling Self-Propelled Motions

Saori Morimoto ^{*}; Makoto Katori [†]; Hiraku Nishimori [‡]

13 February 2025

Abstract

In non-equilibrium statistical physics, active matters in both living and non-living systems have been extensively studied. In particular, self-propelled particle systems provide challenging research subjects in experimental and theoretical physics, since individual and collective behaviors of units performing persistent motions can not be described by usual fluctuation theory for equilibrium systems. A typical example of man-made self-propelled systems which can be easily handled in small-sized experiments is a system of camphor floats put on the surface of water. Based on the experimental and theoretical studied by Nishimori et al. (J. Phys. Soc. Jpn. **86** (2017) 101012), we propose a new type of mathematical models for complex motions of camphor disks on the surface of water. In the previous mathematical models introduced by Nishimori et al. are coupled systems of the equations of motion for camphor disks described by ordinary differential equations and the partial differential equation for the concentration field of camphor molecules in water. Here we consider coupled systems of equation of motions of camphor disks and random walks representing individual camphor molecules in water. In other words, we take into account non-equilibrium fluctuations by introducing stochastic processes into the deterministic models. Numerical simulation shows that our models can represent self-propelled motions of individual camphor disk as well as repulsive interactions among them. We focus on the one-dimensional models in which viscosity is dominant, and derive a dynamical system of a camphor disk by taking the average of random variables of our stochastic system. By studying both of stochastic models and dynamical systems, we clarify the transitions between three phases of motions for a camphor disk depending on parameters.

Keywords: Active matter; Self-propelled interacting particle systems; Camphor float systems; Stochastic models; Dynamical systems

^{*}Department of Physics, Faculty of Science and Engineering, Chuo University, Kasuga, Bunkyo-ku, Tokyo 112-8551, Japan

[†]Department of Physics, Faculty of Science and Engineering, Chuo University, Kasuga, Bunkyo-ku, Tokyo 112-8551, Japan; e-mail: makoto.katori.mathphys@gmail.com

[‡]Meiji Institute for Advanced Study of Mathematical Sciences, Meiji University, Nakano, Nakano-ku, Tokyo 164-8525, Japan; e-mail: nishimor2@meiji.ac.jp

1 Introduction

Although persistent motion is a common feature of living systems, recently several models composing of self-propelled non-living units have been studied to simulate physical and chemical systems. Such *self-propelled particle systems* exhibit many interesting collective motions, which can not be realized as the thermal or chemical fluctuation phenomena in equilibrium systems. Self-propelled particle systems in both living and non-living worlds have been extensively studied in non-equilibrium statistical physics [8].

In order to clarify the fundamental mechanism of individual and cooperative motions of self-propelled particles, artificial systems consisting of easily handled particles shall be studied experimentally and theoretically. As a typical example among various types of man-made self-propelled particles, a system of *camphor floats* put on the surface of water has been widely studied. In particular, a camphor disk is the simplest object which is a circular camphor float [3, 5, 6]. A camphor disk is prepared by soaking a filter paper in camphor solution and drying it. From a camphor disk floated on water, camphor molecules are extended to the water surface, which decreases the surface tension around the disk.

Experimental Observation by Nishimori et al. [5]

Nishimori et al. [5] reported the following observation in experiments, where a camphor disk was floated in a quasi-one-dimensional water channel starting from the rest state. The following are cited from [5].

Initial condition At the initial condition, no camphor molecule is present on a water and camphor disk is set in a stationary state (rest state). Therefore, camphor concentration around the disk increases with time due to the supply of camphor molecules from the disk, which spread out on water and sublimate from the water surface to the air. These three phenomena, i.e., supply, diffusion, and sublimation, make a surface-concentration profile of camphor molecules on water. With an increase in the surface-concentration, the surface tension decreases around the disk. However, the force balance is kept as long as the surface concentration profile is isotropic, and the disk is still stationary.

Perturbation Small perturbations, such as the fluctuation of camphor concentration or Brownian motion of the disk, break the symmetry of the concentration profile, resulting in an imbalance of surface tension acting on the camphor disk. Then, the disk experiences a small driving force toward the lower concentration direction of camphor and begins to migrate with low speed.

Positive feedback The little shift of the disk position enhances the asymmetry of the camphor profile, and thus, the driving force of camphor motion increases. Owing to such a positive feedback process, the initial small perturbation increases with time.

Steady state Finally, the camphor disk achieves steady motion with a terminal velocity, in which the driving force is balanced with the viscosity of water.

Nishimori et al. [5] introduced the following one-dimensional model: Let $x_c(t) \in \mathbb{R}$ be the position of the center of the camphor disk at time $t \geq 0$ and define the velocity by $v_c(t) = dx_c(t)/dt$. The surface-concentration of camphor is described by a field $u(t, x)$, where $(t, x) \in [0, \infty) \times \mathbb{R}$ is the spatio-temporal coordinate. Then the following coupled system of ordinary and partial differential equations was considered;

$$m \frac{dv_c(t)}{dt} = -\mu v_c(t) + \frac{1}{2r} \left[\gamma(u(t, x_c + r)) - \gamma(u(t, x_c(t) - r)) \right], \quad (1.1)$$

$$\frac{\partial u(t, x)}{\partial t} = D \frac{\partial^2 u(t, x)}{\partial x^2} - \kappa u(t, x) + S(x, x_c(t); r), \quad (1.2)$$

where

μ = the friction constant,

$\gamma(u)$ = the surface tension as a function of the camphor concentration field u ,

r = the radius of the camphor disk,

D = effective diffusion constant of camphor on the water surface,

κ = the sum of sublimation constant and dissolution.

$$S(x, x_c(t), r) = \text{the function of the supply rate of camphor from the disk at } x_c(t). \quad (1.3)$$

Nishimori et al. [5] assumed the following for $\gamma(u)$,

$$\gamma(u) = \frac{\gamma_0 - \gamma_1}{(\beta u)^2 + 1} + \gamma_1, \quad (1.4)$$

where β is a positive constant, γ_0 and γ_1 are the surface tensions of pure water and saturated camphor aqueous solution respectively, and

$$S(x, x_c; r) = \begin{cases} S_0, & |x - x_c| \leq r, \\ 0, & |x - x_c| > r, \end{cases} \quad (1.5)$$

where S_0 is the supply rate from the camphor grain to the surface of water. They also used another form for $S(x, x_c; r)$ using the Dirac delta function;

$$S(x, x_c; r) = 2r S_0 \delta(x - x_c). \quad (1.6)$$

Nishimori et al. [5] have assumed that the relaxation rate of $u(t, x)$ in (1.2) is much faster than the acceleration (deceleration) rate of $x_c(t)$ in (1.1). They have considered the case such that the field of camphor surface-concentration $u(t, x)$ relaxes with negligibly short time to the quasi-steady migration state following the quasi-steady movement of the camphor disk with velocity $v_c(t)$.

2 Stochastic Newtonian-Motion model

2.1 Newtonian equation coupled with random walks

In the model system proposed by Nishimori et al. [5], the camphor disk is considered as a macroscopic particle obeying the Newtonian equation (1.1), while the field of camphor surface-concentration $u(t, x)$ follows the diffusion-type equation (1.2).

In the following, we consider a microscopic model for supply, diffusion, and sublimation of camphor molecules on a surface of water by using symmetric random walks which approximate the Brownian motions of camphor molecules in water. We consider the three-dimensional space $\mathbb{R}^3 \ni (x, y, z)$, where the $z = 0$ plane is regarded as the water surface. We represent a camphor disk by a point mass having mass m , which can move on the $z = 0$ plane. The random walks representing the camphor molecules in water are moving only in the region $z \leq 0$.

- (1) We consider a discrete-time model with time $t \in \mathbb{N}_0 := \{1, 2, \dots\}$. The particle (camphor disk) releases N random walkers (camphor molecule) every time t . In the following simulation, we set $N = 50$.

This represents the last term, $S(x, x_c(t); r)$, in the right-hand side of the diffusion-type equation (1.2).

- (2) Each random walker independently performs three-dimensional symmetric random walk in the region $z \leq 0$. Set $m_1 \in \mathbb{N} := \{1, 2, \dots\}$ and let the displacement of each hopping be $1/\sqrt{m_1}$. During the time unit, m_2 steps are performed by each random walker. In the following simulation, we set $m_1 = m_2 = 5$.

This represents the first term, $D\partial^2 u(t, x)/\partial x^2$, in the right-hand side of (1.2).

- (3) Set $q \in [0, 1]$. If a random walker arrives at the $z = 0$ plane, and if it chooses the positive z -direction for a hopping, the hopping is canceled and it remains at the same position in $z = 0$ with probability $1 - q$, and it is annihilated with probability q . In the following simulation, we set $q = 0.3$.

This represents the second term, $-\kappa u(t, x)$, in the right-hand side of (1.2) representing sublimation.

The position of the particle at time t is denoted by $\mathbf{r}(t)$. We write the coordinate at time t of the j -th random walker ($j = 1, 2, \dots, N$) starting from $\mathbf{r}(s)$ at time s as $\mathbf{W}_j^{\mathbf{r}(s)}(t - s)$, $t = \{s, s + 1, \dots\}$. The time when it is annihilated at the $z = 0$ plane is denoted by $\tau_j^{\mathbf{r}(s)} \in \{s + 1, s + 2, \dots, \infty\}$. We think that after this time, the random walk is to be the null state \emptyset ; $\mathbf{W}_j^{\mathbf{r}(s)}(t) \equiv \emptyset$ for $t \geq \tau_j^{\mathbf{r}(s)}$. The empirical measure of random walks at time t is denoted as

$$\Xi_t(\cdot) = \sum_{s=0}^{t-1} \sum_{j=1}^N \mathbf{1}(\tau_j^{\mathbf{r}(s)} > t) \delta_{\mathbf{W}_j^{\mathbf{r}(s)}(m_2(t-s))/\sqrt{m_1}}(\cdot), \quad (2.1)$$

where $\mathbf{1}(\omega)$ denote the indicator function of a condition ω : $\mathbf{1}(\omega) = 1$ if ω is satisfied, $\mathbf{1}(\omega) = 0$ otherwise. Here $\delta_{\mathbf{w}}(\cdot)$ is the point-mass (Dirac) measure located at the position \mathbf{w} , and for any subset $\Omega \subset \mathbb{R}^3$, the equality

$$\int_{\Omega} \delta_{\mathbf{w}}(d\mathbf{r}) = \mathbf{1}(\mathbf{w} \in \Omega) \quad (2.2)$$

is satisfied, where $d\mathbf{r} = dx dy dz$.

- (4) Assume that the position of the camphor disk is $\mathbf{r} = (x, y, z)$. We consider the rectangular parallelepiped regions with sizes

$$L_x = 2, \quad L_y = 2, \quad L_z = 1 \quad (2.3)$$

in the x -, y -, and z -direction, respectively. We set the following four regions around \mathbf{r} ,

$$\begin{aligned} \Lambda_{x+}(\mathbf{r}) &= \{(\xi_1, \xi_2, \xi_3) : x \leq \xi_1 < x + L_x, y - L_y/2 \leq \xi_2 \leq y + L_y/2, -L_z \leq \xi_3 \leq 0\}, \\ \Lambda_{x-}(\mathbf{r}) &= \{(\xi_1, \xi_2, \xi_3) : x - L_x \leq \xi_1 < x, y - L_y/2 \leq \xi_2 \leq y + L_y/2, -L_z \leq \xi_3 \leq 0\}, \\ \Lambda_{y+}(\mathbf{r}) &= \{(\xi_1, \xi_2, \xi_3) : x - L_x/2 \leq \xi_1 \leq x + L_x/2, y \leq \xi_2 < y + L_y, -L_z \leq \xi_3 \leq 0\}, \\ \Lambda_{y-}(\mathbf{r}) &= \{(\xi_1, \xi_2, \xi_3) : x - L_x/2 \leq \xi_1 \leq x + L_x/2, y - L_y \leq \xi_2 < y, -L_z \leq \xi_3 \leq 0\}, \end{aligned} \quad (2.4)$$

and the union of them is written by

$$\Lambda(\mathbf{r}) = \Lambda_{x+}(\mathbf{r}) \cup \Lambda_{x-}(\mathbf{r}) \cup \Lambda_{y+}(\mathbf{r}) \cup \Lambda_{y-}(\mathbf{r}). \quad (2.5)$$

For Ξ_t , the number of random walkers included in each region is given by

$$\begin{aligned} \Xi_t(\Lambda_{\sharp}(\mathbf{r})) &= \int_{\Lambda_{\sharp}(\mathbf{r})} \Xi_t(d\mathbf{r}') \\ &= \int_{\Lambda_{\sharp}(\mathbf{r})} \sum_{s=0}^{t-1} \sum_{j=1}^N \mathbf{1}(\tau_j^{\mathbf{r}(s)} > t) \delta_{\mathbf{W}_j^{\mathbf{r}(s)}(m_2(t-s))/\sqrt{m_1}}(d\mathbf{r}') \\ &= \sum_{s=0}^{t-1} \sum_{j=1}^N \mathbf{1}(\tau_j^{\mathbf{r}(s)} > t) \mathbf{1}(\mathbf{W}_j^{\mathbf{r}(s)}(m_2(t-s))/\sqrt{m_1} \in \Lambda_{\sharp}(\mathbf{r})), \\ &\quad \sharp \in \{x_+, x_-, y_+, y_-\}. \end{aligned} \quad (2.6)$$

Due to the asymmetry of the number of random walkers around the camphor disk, the driving force acts the camphor disk toward the direction of the smaller number of random walkers;

$$\begin{aligned} \mathbf{F}(\mathbf{r}(t), \Xi_t) &= (F_x(\mathbf{r}(t), \Xi_t), F_y(\mathbf{r}(t), \Xi_t)), \\ F_x(\mathbf{r}(t), \Xi_t) &= -\beta \left[\Xi_t(\Lambda_{x+}(\mathbf{r}(t))) - \Xi_t(\Lambda_{x-}(\mathbf{r}(t))) \right], \\ F_y(\mathbf{r}(t), \Xi_t) &= -\beta \left[\Xi_t(\Lambda_{y+}(\mathbf{r}(t))) - \Xi_t(\Lambda_{y-}(\mathbf{r}(t))) \right], \quad t \in \mathbb{N}_0, \end{aligned} \quad (2.7)$$

where β is a positive constant.

This represents the second term, $[\gamma(u(t, x_c + r)) - r(u(t, x_c - r))]/2r$, in the right-hand side of the Newtonian equation (1.1).

- (5) Set the initial state of the camphor disk;

$$\mathbf{r}(0) : \text{initial position}, \quad \mathbf{v}(0) : \text{initial velocity}. \quad (2.8)$$

Notice that both are vectors on the $z = 0$ plane representing the water surface.

- (6) For each discrete time $t \in \mathbb{N}_0$, evolve the position and velocity of camphor disk by the following difference equations,

$$\begin{aligned} m[\mathbf{v}(t+1) - \mathbf{v}(t)] &= -\mu\mathbf{v}(t) + \mathbf{F}(\mathbf{r}(t), \Xi_t), \\ \mathbf{r}(t+1) &= \mathbf{r}(t) + \mathbf{v}(t+1). \end{aligned} \quad (2.9)$$

Remark 1 In the original model by Nishimori et al. [5], the surface tension γ changes depending on the surface-concentration of camphor u by the formula (1.4), and the spatial asymmetry of surface tension causes the driving force of camphor disk as given by the second term of the right-hand side of (1.1). Here we consider a linearization of the surface tension γ of u and then the driving force is assumed to be simply proportional to the spatial asymmetry of the camphor surface-concentration $u(t, x)$ as (2.7).

2.2 Simulation Results

2.2.1 Single camphor disk

First we have simulated the motion of single camphor disk, where we put the initial velocity in the positive x -direction, $\mathbf{v}(0) = (2, 0, 0)$ at $\mathbf{r}(0) = (0, 0, 0)$. Figures 1 and 2 show the position of camphor disk (red disk) and the distribution of random walkers representing the camphor molecules (blue dots) a while later. Here we set $m_1 = m_2 = 3$ and $\beta/\mu = 0.05$. Other parameters are the same as mentioned above. As shown by figures, the density of random walkers has higher value in the left (backward) than in the right (forward) of the camphor disk. Hence the driving force of camphor disk is in the right direction and the disk will continue its motion to the right.

By the density fluctuation of random walkers, the velocity of camphor disk becomes to have y -component as shown by Fig. 2.

2.2.2 Two camphor disks

Next we put two camphor disks in the x -axis with a small distance; $\mathbf{r}_1(0) = (0, 0, 0)$ and $\mathbf{r}_2(0) = (5, 0, 0)$. We set the initial velocities as $\mathbf{v}_1(0) = \mathbf{v}_2(0) = (2, 0, 0)$. Figures 3 and 4 show the positions of two camphor disks (red and green disks) and distribution of random walkers (blue dots) a while later. We can observe a repulsive behavior of two disks, and then they move to the different directions as shown by Fig. 4.

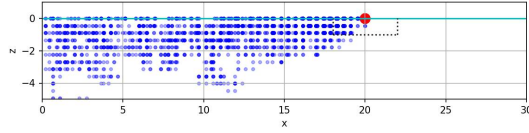


Figure 1: Single camphor disk (red disk) and random walkers representing camphor molecules (blue dots) in the (x, z) -plane. The dotted rectangular around the red disk indicates $\Lambda(\mathbf{r})$.

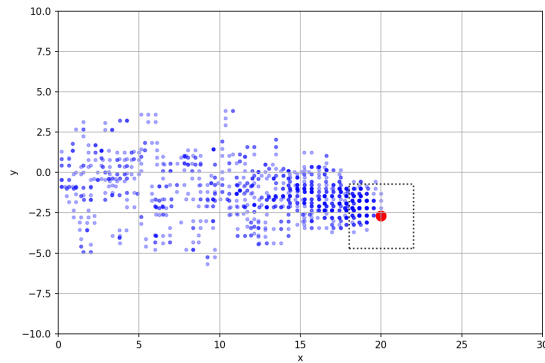


Figure 2: Single camphor disk (red disk) and random walkers representing camphor molecules (blue dots) in the (x, y) -plane. The dotted square around the red disk indicates $\Lambda(\mathbf{r})$.

2.2.3 Three and four camphor disks

We set three (resp. four) camphor disks to make an equilateral triangle (resp. a square). We put appropriate initial velocities to make them collide at the center of the triangle or square. We have observed that the camphor disks show repulsive interaction and they are scattered from each other.

3 Stochastic Viscous-Motion Models and Dynamical Model in One-Dimension

Here we consider the one-dimensional case in order to simplify the analysis and clarify the essential aspects of the present modeling.

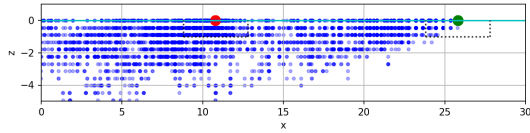


Figure 3: Two camphor disks (red and green disks) and random walkers representing camphor molecules (blue dots) in the (x, z) -plane.

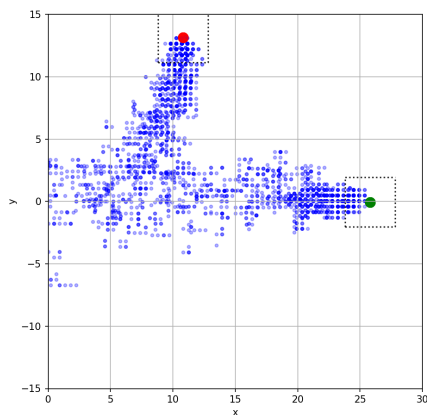


Figure 4: Two camphor disks (red and green disks) and random walkers representing camphor molecules (blue dots) in the (x, y) -plane.

3.1 Stochastic models

When the friction constant μ is large, acceleration is suppressed and the left-hand side of (2.9) will be negligible. In such a case dominated by viscosity, we consider the system

$$v(t+1) = \frac{1}{\mu} F(x(t), \Xi_t), \quad (3.1)$$

$$x(t+1) = x(t) + v(t+1), \quad t \in \mathbb{N}_0, \quad (3.2)$$

which we call the *stochastic viscous-motion model*. Equation (3.1) is written as

$$\begin{aligned}
v(t+1) &= -\frac{\beta}{\mu} \left[\Xi_t(\Lambda_{x^+}(x(t))) - \Xi_t(\Lambda_{x^-}(x(t))) \right] \\
\iff v(t+1) &= -\frac{\beta}{\mu} \sum_{s=0}^{t-1} \left[\sum_{j=1}^N \mathbf{1}(\tau_j^{x(s)} > t) \mathbf{1} \left(\frac{1}{\sqrt{m_1}} W_j^{x(s)}(m_2(t-s)) \in [x(t), x(t) + L_x] \right) \right. \\
&\quad \left. - \sum_{j=1}^N \mathbf{1}(\tau_j^{x(s)} > t) \mathbf{1} \left(\frac{1}{\sqrt{m_1}} W_j^{x(s)}(m_2(t-s)) \in [x(t) - L_x, x(t)] \right) \right], \quad (3.3)
\end{aligned}$$

$t \in \mathbb{N}_0$. We will consider the simple case

$$\mathbf{1}(\tau_j^{x(s)} > t) = \begin{cases} 1, & \text{if } s = t-1, \\ 0, & \text{otherwise.} \end{cases} \quad (3.4)$$

That is, the random walkers survive (the camphor molecules stay in water avoiding from sublimation to the air) only for the time unit) In this case, we have

$$\begin{aligned}
v(t+1) &= -\frac{\beta}{\mu} \left[\sum_{j=1}^N \mathbf{1} \left(\frac{1}{\sqrt{m_1}} W_j^{x(t-1)}(m_2) \in [x(t), x(t) + L_x] \right) \right. \\
&\quad \left. - \sum_{j=1}^N \mathbf{1} \left(\frac{1}{\sqrt{m_1}} W_j^{x(t-1)}(m_2) \in [x(t) - L_x, x(t)] \right) \right], \\
x(t+1) &= x(t) + v(t+1), \quad t \in \mathbb{N}_0. \quad (3.5)
\end{aligned}$$

3.1.1 Brownian motion limit

In the following limit, the scaled random walk converges to the one-dimensional standard Brownian motion in probability; for a given initial position $x \in \mathbb{R}$,

$$\left(\frac{1}{\sqrt{m_1}} W^x(m_2 t) \right)_{t \geq 0} \longrightarrow \left(\sqrt{2D} B^x(t) \right)_{t \geq 0} \quad \text{as } m_1, m_2 \rightarrow \infty \quad \text{with } \frac{m_2}{m_1} \rightarrow 2D, \quad (3.6)$$

where $(B^x(t))_{t \geq 0}$ denotes the one-dimensional standard Brownian motion started from x . In such a *diffusion scaling limit*, Eq. (3.3) is reduced to

$$\begin{aligned}
v(t+1) &= -\frac{\beta}{\mu} \sum_{s=0}^{t-1} \left[\sum_{j=1}^N \mathbf{1}(\tau_j^{x(s)} > t) \mathbf{1} \left(\sqrt{2D} B_j^{x(s)}(t-s) \in [x(t), x(t) + L_x] \right) \right. \\
&\quad \left. - \sum_{j=1}^N \mathbf{1}(\tau_j^{x(s)} > t) \mathbf{1} \left(\sqrt{2D} B_j^{x(s)}(t-s) \in [x(t) - L_x, x(t)] \right) \right], \quad t \in \mathbb{N}_0. \quad (3.7)
\end{aligned}$$

Here $\tau_j^{x(s)}$ denote the time that the limit Brownian motion $(B^{x(s)}(t))_{t \geq 0}$ is annihilated. The position of camphor disk is moving as

$$x(t+1) = x(t) + v(t+1), \quad t \in \mathbb{N}_0. \quad (3.8)$$

3.1.2 Mean-value motion

Now we take the mean values with respect to the Brownian motions,

$$\begin{aligned} \langle v(t+1) \rangle = & -\frac{\beta}{\mu} \sum_{s=0}^{t-1} \left[\sum_{j=1}^N \left\langle \mathbf{1}(\tau_j^{x(s)} > t) \mathbf{1} \left(\sqrt{2D} B_j^{x(s)}(t-s) \in [x(t), x(t) + L_x] \right) \right\rangle \right. \\ & \left. - \sum_{j=1}^N \left\langle \mathbf{1}(\tau_j^{x(s)} > t) \mathbf{1} \left(\sqrt{2D} B_j^{x(s)}(t-s) \in [x(t) - L_x, x(t)] \right) \right\rangle \right], \quad (3.9) \end{aligned}$$

The transition probability density of the one-dimensional standard Brownian motion is given by

$$p(t, y|x) = \frac{1}{\sqrt{2\pi t}} e^{-(y-x)^2/2t}, \quad t > 0, \quad x, y \in \mathbb{R}. \quad (3.10)$$

Then, provided $x(s) \in \mathbb{R}$, $s = 0, 1, \dots, t-1$, the right-hand side of (3.9) will be written as

$$-N \frac{\beta}{\mu} \sum_{s=0}^{t-1} G(t-s) \left[\int_{x(t)}^{x(t)+L_x} p(2D(t-s), x|x(s)) dx - \int_{x(t)-L_x}^{x(t)} p(2D(t-s), x|x(s)) dx \right], \quad (3.11)$$

where we have assumed independence of the annihilation process of Brownian motion and its position, and defined the function

$$G(t-s) := \langle \mathbf{1}(\tau^{x(s)} > t) \rangle, \quad t > s, \quad (3.12)$$

which corresponds to the survival probability of the camphor molecule in water avoiding from sublimation for time period $t-s$. We call (3.12) the *sublimation function*. If $L_x \ll 1$, the above will be written as

$$\begin{aligned} & -N \frac{\beta L_x}{\mu} N \sum_{s=1}^{t-1} G(t-s) \left[p(2D(t-s), x(t) + L_x/2|x(s)) - p(2D(t-s), x(t) - L_x/2|x(s)) \right] \\ & \quad + O(L_x^2) \\ = & -N \frac{\beta L_x^2}{\mu} \sum_{s=1}^{t-1} G(t-s) \frac{p(2D(t-s), x(t) + L_x/2|x(s)) - p(2D(t-s), x(t) - L_x/2|x(s))}{L_x} \\ & \quad + O(L_x^2) \quad (3.13) \end{aligned}$$

We take the following scaling limit,

$$N \rightarrow \infty, \quad L_x \rightarrow 0 \quad \text{with} \quad N \frac{\beta L_x^2}{\mu} \rightarrow \alpha \ell, \quad (3.14)$$

where $0 < \alpha\ell < \infty$. Then (3.13) will converge to

$$-\alpha\ell \sum_{s=1}^{t-1} G(t-s) \frac{\partial}{\partial x} p(2D(t-s), x|x(s)) \Big|_{x=x(t)}. \quad (3.15)$$

The above calculation implies the *Markov chain*

$$(x(t), v(t)) \rightarrow (x(t+1), v(t+1)), \quad t \in \mathbb{N}_0. \quad (3.16)$$

with

$$\begin{aligned} v(t+1) &= -\alpha\ell \sum_{s=1}^{t-1} G(t-s) \frac{\partial}{\partial x} p(2D(t-s), x|x(s)) \Big|_{x=x(t)}, \\ x(t+1) &= x(t) + v(t+1). \end{aligned} \quad (3.17)$$

Two examples of sublimation function G are given by

$$G(u) = e^{-\kappa u}, \quad u > 0. \quad (3.18)$$

and

$$G(u) = \begin{cases} 1, & \text{if } u = 1, \\ 0, & \text{if } u > 1. \end{cases} \quad (3.19)$$

The former corresponds to the second term, $-\kappa u(t, x)$, in the right-hand side of (1.1) of the model by Nishimori et al. [5].

3.2 Dynamical system

From now on, we will consider the simple case with (3.19) for the sublimation function. Then (3.17) gives the following deterministic system with discrete-time, which we simply call the *dynamical system*,

$$v(t+1) = -\alpha\ell \frac{\partial}{\partial x} p(2D, x|x(k)) \Big|_{x=x(t)}, \quad (3.20)$$

$$x(t+1) = x(t) + v(t+1), \quad t \in \mathbb{N}_0. \quad (3.21)$$

The right-hand side of (3.20) is calculated as

$$\begin{aligned} & -\alpha\ell \frac{\partial}{\partial x} \frac{1}{\sqrt{4\pi D}} e^{-(x-x(n-1))^2/4D} \Big|_{x=x(n)} \\ &= -\frac{\alpha\ell}{\sqrt{4\pi D}} \left(-\frac{2(x-x(n-1))}{4D} \right) e^{-(x-x(n-1))^2/4D} \Big|_{x=x(n)} \\ &= \frac{\alpha\ell}{4\sqrt{\pi D^{3/2}}} (x(n) - x(n-1)) e^{-(x(n)-x(n-1))^2/4D}. \end{aligned}$$

By (3.21),

$$x(n) - x(n-1) = v(n).$$

Then the time-evolution equation of velocity is given by the following iterative equation,

$$v(n+1) = \frac{\alpha\ell}{4\sqrt{\pi}D^{3/2}}v(n)e^{-v(n)^2/4D}, \quad n \in \mathbb{N}_0. \quad (3.22)$$

3.2.1 Analysis of dynamical system

Set

$$V(n) := \frac{v(n)}{2\sqrt{D}}, \quad n \in \mathbb{N}_0, \quad (3.23)$$

and

$$C := \frac{4\sqrt{\pi}D^{3/2}}{\alpha\ell} > 0. \quad (3.24)$$

Then (3.22) is written as

$$\frac{v(n+1)}{2\sqrt{D}} = \frac{\alpha\ell}{4\sqrt{\pi}D^{3/2}} \frac{v(n)}{2\sqrt{D}} e^{-(v(n)/2\sqrt{D})^2} \iff CV(n+1) = F(V(n)), \quad n \in \mathbb{N}_0 \quad (3.25)$$

with

$$F(x) = xe^{-x^2}. \quad (3.26)$$

Remark 2 If we take the square of (3.25), we obtain

$$C^2V(n+1) = V(n)^2e^{-2V(n)^2} \iff -2C^2V(n+1) = -2V(n)^2e^{-2V(n)^2}.$$

Let

$$Y(n) := -2V(n)^2 \leq 0. \quad (3.27)$$

Then we have

$$C^2Y(n+1) = Y(n)e^{Y(n)}, \quad n \in \mathbb{N}_0. \quad (3.28)$$

Here we consider the *Lambert W function* (see, for instance, [7]). This function is defined as the inverse function of the mapping

$$x \mapsto xe^x.$$

This mapping is not injective, and the Lambert W function has two branches with a branching point at $(-e^{-1}, -1)$ in the plane $(x, W) \in \mathbb{R}^2$. The upper branch is denoted by $W_0(x)$ defined for $x \in [-e^{-1}, \infty)$. By this definition, we can show that

$$W_0(x)e^{W_0(x)} = x, \quad W_0(0) = 0, \quad W_0(e) = 1,$$

and $W_0(x) \simeq x$ as $x \rightarrow 0$. Another branch is denoted by $W_{-1}(x)$. See [1] for more details. Using the Lambert W function, (3.28) is written as

$$W(C^2Y(n+1)) = Y(n), \quad n \in \mathbb{N}_0. \quad (3.29)$$

Fixed points

If we write the stationary solution of (3.25) as $V_* = v_*/(2\sqrt{D})$, then we have

$$CV_* = V_*e^{-V_*^2}. \quad (3.30)$$

It has a trivial solution

$$V_* = 0 \quad \Longleftrightarrow \quad v_* = 0. \quad (3.31)$$

The non-zero solutions should satisfy

$$C = e^{-V_*^2}. \quad (3.32)$$

If and only if $C < 1$, non-zero solution exists. Assume $C < 1$. Then (3.32) have solutions

$$\begin{aligned} \log C = -V_*^2 &\Longleftrightarrow V_* = \pm\sqrt{-\log C} \\ &\Longleftrightarrow v_* = \pm 2\sqrt{D}V_* = \pm 2\sqrt{-D \log C}. \end{aligned} \quad (3.33)$$

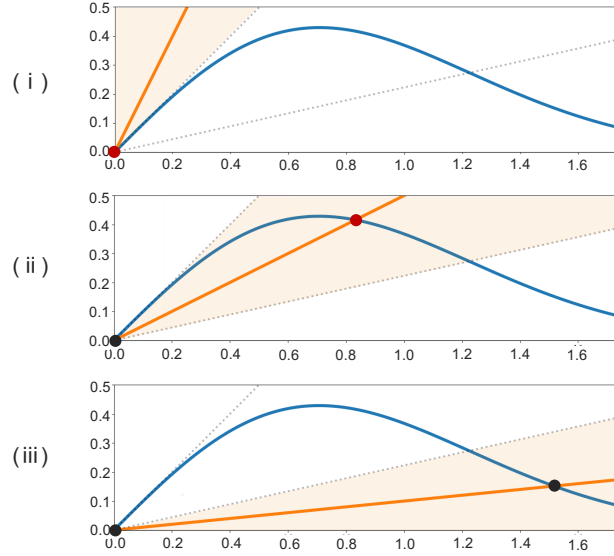


Figure 5: The functions $y = F(x)$ given by (3.26) and $y = Cx$ are drawn by a blue curve and a red line, respectively for three cases. (i) $C \geq 1$, (ii) $e^{-1} < C < 1$, and (iii) $0 < C < e^{-1}$. The stable (resp. unstable) fixed points are indicated by red (resp. black) dots.

Linear stability

We can prove the following by the linear stability analysis. See Fig. 5.

Proposition 3.1 (i) *Assume*

$$C \geq 1 \iff \frac{4\sqrt{\pi}D^{3/2}}{\alpha\ell} \geq 1.$$

Then the stationary solution is uniquely given by

$$V_* = 0 \iff v_* = 0.$$

The zero solution $v_ = 0$ (the rest state) is stable.*

(ii) *Assume*

$$e^{-1} = 0.3678\dots < C < 1 \iff e^{-1} < \frac{4\sqrt{\pi}D^{3/2}}{\alpha\ell} < 1.$$

Then there are three stationary solutions

$$V_* = 0 \text{ and } \pm V_* = \pm\sqrt{-\log C} \iff v_* = 0 \text{ and } v_* = \pm 2\sqrt{-D \log C}.$$

The zero solution $v_ = 0$ is unstable and the non-zero solutions $v_* = \pm 2\sqrt{-D \log C}$ (the steady motions) are stable.*

(iii) *Assume*

$$0 < C < e^{-1} \iff 0 < \frac{4\sqrt{\pi}D^{3/2}}{\alpha\ell} < e^{-1}.$$

Then there are three stationary solutions

$$V_* = 0 \text{ and } \pm V_* = \pm\sqrt{-\log C} \iff v_* = 0 \text{ and } v_* = \pm 2\sqrt{-D \log C}.$$

Both of the zero solution $v_ = 0$ and the non-zero solutions $v_* = \pm 2\sqrt{-D \log C}$ are unstable and oscillatory motion will be observed.*

Proof Let

$$V(n) = V_* + \varepsilon \text{ with } |\varepsilon| \ll 1. \quad (3.34)$$

Then by the equation of motion (3.25),

$$\begin{aligned} V(n+1) &= \frac{1}{C}V(n)e^{-V(n)^2} \\ &= \frac{1}{C}(V_* + \varepsilon)e^{-(V_* + \varepsilon)^2} \\ &= \frac{1}{C}V_*e^{-V_*^2} + \frac{1}{C}e^{-V_*^2}(1 - 2V_*^2)\varepsilon + O(\varepsilon^2). \end{aligned}$$

By (3.30), we have

$$V(n+1) = V_* + \frac{1}{C}e^{-V_*^2}(1 - 2V_*^2)\varepsilon + O(\varepsilon^2). \quad (3.35)$$

We define

$$\lambda := \lim_{\varepsilon \downarrow 0} \frac{V(n+1) - V_*}{V(n) - V_*}. \quad (3.36)$$

Then (3.35) gives

$$\lambda = \lim_{\varepsilon \downarrow 0} \frac{1}{\varepsilon} \left[\frac{1}{C} e^{-V_*^2} (1 - 2V_*^2) \varepsilon + O(\varepsilon^2) \right] = \frac{1}{C} e^{-V_*^2} (1 - 2V_*^2). \quad (3.37)$$

By definition (3.36), we can say that for infinitesimal perturbation

$$\begin{aligned} |\lambda| < 1 &\iff V_* \text{ is stable,} \\ |\lambda| > 1 &\iff V_* \text{ is unstable.} \end{aligned} \quad (3.38)$$

For $V_* = 0$, (3.37) gives

$$\lambda = \frac{1}{C}. \quad (3.39)$$

Then

$$\begin{aligned} C > 1 &\implies V_* = 0 \text{ is stable,} \\ 0 < C < 1 &\implies V_* = 0 \text{ is unstable.} \end{aligned} \quad (3.40)$$

For $V_* = \pm\sqrt{-\log C}$, (3.37) gives

$$\lambda = \frac{1}{C} \times C(1 + 2 \log C) = 1 + 2 \log C. \quad (3.41)$$

Then

$$\begin{aligned} e^{-1} < C < 1 &\iff -1 < \lambda < 1 \implies V_* = \pm\sqrt{-\log C} \text{ is stable,} \\ 0 < C < e^{-1} &\iff \lambda < -1 \implies V_* = \pm\sqrt{-\log C} \text{ is unstable.} \end{aligned} \quad (3.42)$$

Then the proof is complete. ■

3.3 Comparison between stochastic models and dynamical systems

Here we compare the results of numerical simulation of the simple case of stochastic viscous-motion models (3.5) in Section 3.1 and the corresponding dynamical systems (3.22) in Section 3.2. In the former, we define the parameter

$$\widehat{\ell} := \frac{\beta L_x^2}{\mu}. \quad (3.43)$$

Other parameters are set as mentioned in Section 2.1; $N = 50$, $m_1 = m_2 = 5$, and $L_x = 2$. In the latter, we set

$$\alpha = N = 50, \quad D = \frac{m_2}{2m_1} = \frac{1}{2}, \quad (3.44)$$

and change the parameter ℓ . In this case, (3.24) gives

$$C = \frac{\sqrt{2\pi}}{50\ell} \doteq 5.0 \times 10^{-2} \times \frac{1}{\ell}. \quad (3.45)$$

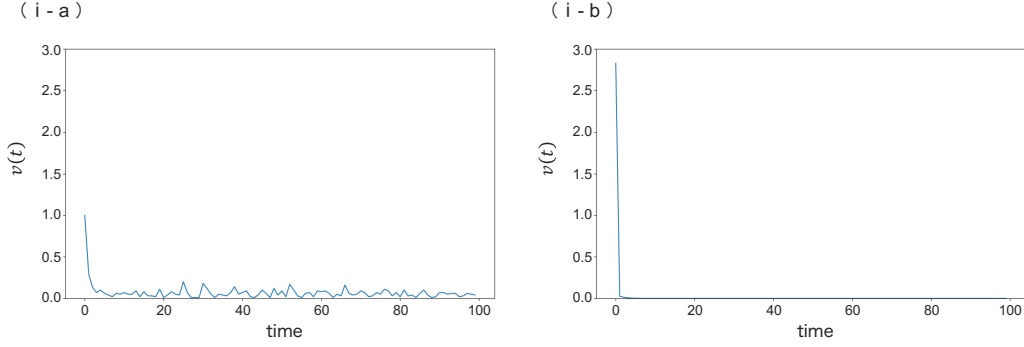


Figure 6: Comparison between the the simple case of stochastic viscous-motion model (3.5) and the dynamical system (3.22). (i-a) for the stochastic model with $\hat{\ell} = 0.04$ and (ii-b) for the dynamical system with $\ell = 0.01$.

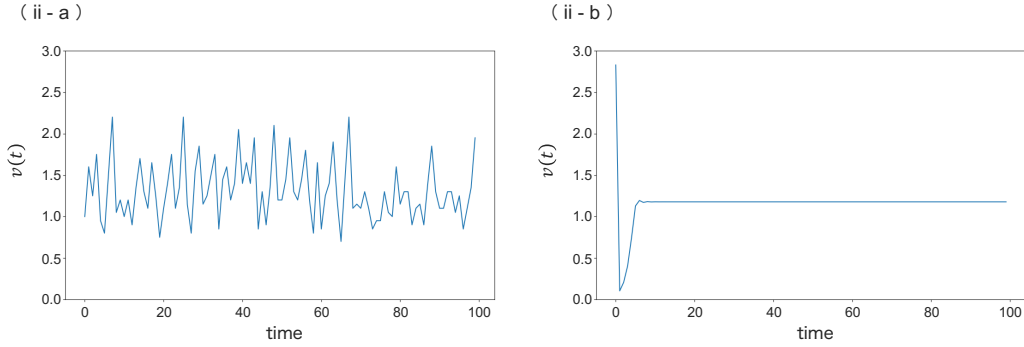


Figure 7: Comparison between the the simple case of stochastic viscous-motion model (3.5) and the dynamical system (3.22). (ii-a) for the stochastic model with $\hat{\ell} = 0.2$ and (ii-b) for the dynamical system with $\ell = 0.1$.

In Figs. 6–8 we show the time evolution of the velocity $v(t)$ for the stochastic viscous-motion models starting from $v(0) = 1$ in the left three figures (in the time unit T_1), and for the dynamical systems starting from $v(0) = 2\sqrt{2}$. in the right three figures. The parameters are shown in the caption. Notice that for the dynamical systems, $\ell = 0.01$ in Fig. 6 (i-b) gives $C \cong 5$ which satisfies the condition of the case (i) in Proposition 3.1, $\ell = 0.1$ in Fig. 7 (ii-b) gives $C \cong 0.5$ which satisfies the condition of the case (ii) in Proposition 3.1, and $\ell = 0.5$ in Fig. 8 (iii-b) gives $C \cong 0.1$ which satisfies the condition of the case (iii) in Proposition 3.1. Figure 6 (i-a) and (i-b) show that the rest state $v(t) = 0$ is stable, and Fig 7 (ii-a) and (ii-b) show that the systems have the non-zero velocity states $v(t) \neq 0$ as the steady state. On the other hand, Fig 8 (iii-a) and (iii-b) show oscillatory behavior of motions between $v = 0$ state and $v \neq 0$ state. In summary, the transitions between the three different phases of motions are well-described by the dynamical systems (3.22), and the stochastic viscous-motion models can show fluctuations around the solutions of the dynamical system.

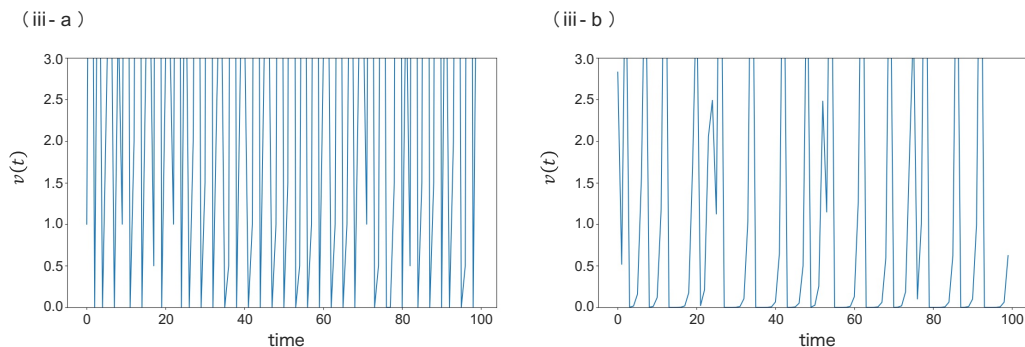


Figure 8: Comparison between the the simple case of stochastic viscous-motion model (3.5) and the dynamical system (3.22). (iii-a) for the stochastic model with $\hat{\ell} = 2$ and (iii-b) for the dynamical system with $\ell = 0.5$.

4 Concluding Remarks and Future Problems

We list out the remarks and future problems.

- (i) We have analyzed the stochastic models and the dynamical systems in the viscosity dominated cases for one camphor disk. The time evolution of the mean values of velocity is well described by the dynamical system for each values of parameters. The fluctuations around the mean values simulated by the stochastic models shall be studied systematically to clarify the parameter dependence of the distribution of deviations from mean values. Moreover, systems including two or more than two disks in one-dimension should be analyzed in order to understand the interactions among camphor disks though the camphor molecules in water which are simulated by random walks in the present stochastic models. The effect of acceleration and deceleration will be studied by the stochastic Newtonian-motion models introduced in Section 2.1. In Section 3.3, we fixed parameters different from $\hat{\ell} = \beta L_x^2 / \mu$. More systematic study on the parameter dependence should be studied.
- (ii) As demonstrated in Section 2.2, two- and three-dimensional systems including many camphor disks seem to be quite interesting. The simulations of the proposed stochastic Newtonian-motion models shall be done and the results should be compared with the experiments reported by the literature [3, 5, 6]. In particular, setting of proper boundary conditions, e.g., a circular boundary condition with changing radius, will be important to make comparison between the experimental results and the theoretical study using stochastic and dynamical systems.

In the present work, we have concentrated on the motions of camphor disks interacting though heterogeneous concentration-field of camphor molecules. Here the filed of camphor molecules is generated and changed by the camphor disks and also the time-evolution of the filed affects the motion of camphor disks. Such feedback effects are common in self-propelled

systems. In the present case, the field causes the repulsive interaction among disks [3, 5, 6], but we will be able to apply the present models to the self-propelled particle systems with attractive interactions. We are considering the possibility to apply our models to study the collective motions of the eusocial insects, in particular, of ants [2, 4]. Another possibility is to apply the present study to the traffic flow and jam problems, where the road conditions and interaction between drivers shall be expressed by the heterogeneous and time-dependent field around cars.

References

- [1] Corless, R. M., Gonnet, G. H., Hare, D. E. G., Jeffrey, D. J., Knuth, D. E.: On the Lambert W function. *Adv. Comput. Math.* **5**, 329-359 (1996)
- [2] Ezoe, A., Morimoto, S., Tanaka, Y., Katori, M., Nishimori, H., Switching particle systems for foraging ants showing phase transitions in path selections, *Physica A* **643** (2024) 129798 (13 pages)
- [3] Matsuda, Y., Ikura, Y., Nishimori, H., Suematsu, N.: Dynamical quorum sensing in non-living active matter. *J. Phys. Soc. Jpn.* **88**, 093002 (2019)
- [4] Morimoto, S., Katori, M., Nishimori, H.: Path annihilation as non-equilibrium phase transition into absorbing state, in preparation
- [5] Nishimori, H., Suematsu, N. J., Nakata, S.: Collective behavior of camphor floats migrating on the water surface. *J. Phys. Soc. Jpn.* **86**, 101012 (2017)
- [6] Suematsu, N., Tatenno, K., Nakata, S., Nishimori H.: Synchronized intermittent motion induced by the interaction between camphor disks. *J. Phys. Soc. Jpn.* **84**, 034802 (2015)
- [7] Veberic, D.: Lambert W function for applications in physics. *Comput. Phys. Commun.* **183**, 2622–2628 (2012); [arXiv:cs.MS/1209.0735](https://arxiv.org/abs/cs/0507035)
- [8] Vicsek, T. Zafeiris, A.: Collective motion. *Phys. Rep.* **517** (2012) 71–140.